Composite Structures 337 (2024) 118062

Contents lists available at ScienceDirect

Composite Structures

journal homepage: www.elsevier.com/locate/compstruct

Connectivity patterns in lead-free piezocomposites: A critical analysis for 0-3 and 1-3 configurations

Francisco J. Cañamero [a,b], Federico C. Buroni [c], Luis Rodríguez-Tembleque [a,*]

[a] Department of Continuum Mechanics and Structures, Escuela Técnica Superior de Ingeniería, Universidad de Sevilla, Camino de los Descubrimientos s/n, Sevilla, 41092, Spain

[b] Fundación Centro Tecnológico Metalmecánico y del Transporte, Parque Empresarial Santana, Linares 23700, Spain

[c] Department of Mechanical Engineering and Manufacturing, Escuela Técnica Superior de Ingeniería and Escuela Politécnica Superior, Universidad de Sevilla, Camino de los Descubrimientos s/n, 41092, Seville, Spain

ARTICLE INFO

Keywords:
BTO piezocomposites
KNN piezocomposites
Mori–Tanaka
Numerical homogenization
Carbon nanotubes
Effective figures of merits

ABSTRACT

In the quest for eco-friendly alternatives within materials science, the development of sustainable and non-toxic piezoelectric composites is of utmost importance. This study undertakes a computational exploration to elucidate the influence of phase connectivity on the engineering performance of lead-free piezocomposites. Employing a combination of analytical and numerical methodologies, we critically evaluated various figures of merit across different microstructural configurations, juxtaposing these findings with traditional lead zirconate titanate (PZT)-based materials. Our analysis considers 0-3 and 1-3 connectivity patterns, incorporating active phases in the form of spherical particles and cylindrical fibers. We also examine the impact of carbon nanotubes (CNTs) in enhancing the polymeric matrix, which introduces the potential for network percolation and further mechanical and electrical property optimization. The study yields pivotal insights into the phase connectivity of lead-free piezocomposites, with direct implications for their application in sensing, actuating, and energy harvesting domains. We ascertain that the electromechanical performance of these composites is contingent upon the connectivity pattern and the proportion of active phase. Notably, the KNNS-BNZH & Polyethylene composite demonstrates exceptional potential in 1-3 configurations, while the BTO & PVDF composite distinguishes itself with superior dielectric and piezoelectric responses across varying volume fractions. The strategic infusion of CNTs into the PDMS matrix emerges as a significant enhancer of electromechanical attributes, albeit with performance improvements that are specific to the type of coefficient and CNT concentration. This investigation underscores the nuanced interplay between composite design and microstructural attributes, reinforcing the critical role these factors play in the advancement of effective and eco-conscious piezoelectric materials.

1. Introduction

Eco-friendly and lead-free piezoelectric materials have recently begun to be studied and have undergone a remarkable development in recent years [1,2]. In the last decade, environmental concerns have led to attempts to eliminate lead-based materials from consumer items, including piezoelectric transducers, sensors and actuators. Regulatory frameworks, such as the Restriction of Hazardous Substances (RoHS) directive in the European Union, are already in place and anticipate the phasing out of lead in electronics, further underscoring the urgency for viable lead-free alternatives. Therefore, the market for lead-free piezoelectric materials and devices is expected to grow in the coming years, driven by increasing demand for environmentally friendly and safe technologies as well as the growing adoption of piezoelectric devices. The main drawback in the adoption of lead-free piezocomposites is the low electro-mechanical performance when compared with their lead-based counterparts. In short, reliable adoption of eco-friendly piezocomposites requires profound understanding of any relevant feature or mechanism that improves coupling performance.

In the realm of piezocomposite materials, the configuration of phase connectivity plays a pivotal role in determining the material's overall performance characteristics. Ten significant connectivity patterns exist in two-phase composites, spanning from a 0-0 unconnected checkerboard arrangement to a 3-3 configuration where both phases are three-dimensionally self-connected. In particular, two of them deserve specific attention, namely 1-3 and 0-3 connectivity patterns, which present

* Corresponding author.
E-mail address: luisroteso@us.es (L. Rodríguez-Tembleque).

https://doi.org/10.1016/j.compstruct.2024.118062
Received 6 December 2023; Received in revised form 31 January 2024; Accepted 21 March 2024
Available online 24 March 2024

distinct advantages and limitations [3,4]. In a 1-3 connectivity, piezoelectric fibers are embedded in a polymer matrix in such a way that the soft polymer matrix has sufficient ductility to sustain mechanical deformation and transfer loads to the piezoceramic fibers. This offers high anisotropic properties and, according to Smith [5] and Kumar et al. [6], finds extensive use in aerospace, naval, or biomedical industries. Conversely, the 0-3 connectivity typically involves a random dispersion of piezoelectric particles within the matrix, resulting in isotropic properties but often at the cost of reduced electromechanical coupling [7]. This configuration is typical for active printable piezocomposites [8,9]. The choice between connectivity patterns is not merely a matter of material design but has far-reaching implications in specific engineering applications, such as sensing, actuating, and energy harvesting [10]. Therefore, a rigorous study that elucidates the contrasts in coupling performance between these configurations is not only timely, but also essential for the advancement of efficient piezocomposite materials.

The relations between the microgeometric configurations in piezocomposite systems and these specific applications have been deeply explored in lead-based piezoelectric composites for forty years. In the context of connectivity in piezoelectrics, the pioneering study by Newnham et al. [3] deserves to be mentioned, where the critical role of connectivity patterns in diphasic solids has been firstly elucidated. The work further explored the implications of these patterns for piezoelectric transducers and pyroelectric detectors, offering valuable insights into the structure–property relations in both composite and single-phase materials. Particularly noteworthy is their conclusion that anisotropic structures with a molecular mechanism for piezoelectricity are optimal for hydrostatic sensors, a finding that has had enduring relevance in the field. Later, many experimental [11] and numerical [12–23] works were developed to evaluate the effective properties and the so-called figures of merit (FOMs) to assess their performance for sensing, actuating, or energy harvesting applications.

A recent and comprehensive review on composite connectivity in piezocomposite design can be found in [10]. This review elucidates the different types of connectivity class and their implications on the composite properties. The authors also provide in-depth analysis of the contributions from active and passive phases, focusing primarily on ferroelectric ceramics and polymer-based composites. However, the review does not discuss the environmental impact, particularly the urgent need to transition to lead-free piezoelectrics to mitigate ecological risks and comply with international regulations. This omission is a significant gap that deserves immediate attention for eco-friendly next generation technologies.

Recent works [24–31] have studied lead-free piezocomposites — based on barium titanate ($BaTiO_3$, referred to as BTO) inclusions 1-3-connected to a polydimethylsiloxane (PDMS) or a polyvinylidene fluoride (PVDF) matrix [32,33]– via numerical analysis to study the impact of several microstructural characteristics in improving the performance of such lead-free piezoelectric composites (e.g., the role of tuning the dielectric environment of the matrix by adding nanoinclusions, such as graphene or carbon nanotubes (CNTs)). However, these studies [24–26] were developed considering 2D finite element models, where some important simplifications are assumed. Specifically, intrinsic three-dimensional pattern connectivities, such as the 0-3 configurations, cannot be properly modeled under the plane hypothesis. In contrast, recent 3D representative volume element (RVE) modeling studies — based on the finite element method (FEM)– performed in [7,34] have been shown to be more precise to identify how the CNTs addition to the piezocomposite matrix can affect the piezoelectric performance.

In this context, this work presents a detailed study on the performance of several lead-free piezocomposites, taking into account not only the phase connectivity but also micromechanical aspects, such as active phase volume fraction or matrix tuning. The piezoelectric composites considered in this work are three: BTO embedded in soft polymeric matrices, such as PDMS or PVDF –i.e., BTO & PDMS and BTO & PVDF [11,16,35]– and a potassium sodium niobate (K_{1-x},$Na_x NbO_3$, referred to as KNN) based piezocomposite, i.e., KNNS-BNZH & Polyethylene [36]. This last piezocomposite is based on a lead-free piezoelectric ceramic (KNNS-BNZH) where KNNS means a potassium sodium niobate containing antimony (Sb), and BNZH denotes doping with Bismuth (Bi), Sodium (Na), Zirconium (Zr), and Hafnium (Hf): $0.965(K_{0.48}Na_{0.52})(Nb_{0.96}Sb_{0.04})O_3$-$0.035Bi_{0.5}Na_{0.5}Zr_{0.15}Hf_{0.75}O_3$. For this purpose, this work develops a numerical/analytical microelectromechanical model that helps to elucidate the influence of connectivity patterns in the performance of lead-free piezocomposites for each relevant engineering application. Consequently, various FOMs for actuating, sensing and energy harvesting are analyzed to show if the performance of these lead-free piezoelectric composites present a response compared to the lead-based counterparts.

This paper is organized as follows. Section 2 presents a brief description of the constitutive equations for piezoelectric materials and the computational methods (i.e., Mori–Tanaka and RVE-FEM-based methodologies) to obtain the effective properties of the piezocomposites. Section 3 presents and analyses several effective figures of merit for various combinations of lead-free piezocomposites under 0-3 and 1-3 connectivities. Furthermore, the role of CNT polymeric matrix tuning in lead-free piezocomposites is analyzed on a BTO & PDMS piezocomposite. Finally, the main concluding remarks are presented in Section 4.

2. Micromechanics modeling

In this section, we systematically explore the micromechanical modeling of piezoelectric composites. We start by establishing the constitutive equations that define the electro-mechanical interactions, both at the micro- and macro-scale levels. Two models are used for the estimation of effective coupled properties. It is pertinent to note that both models operate under the assumption of scale separation. Firstly, we present the analytical framework employing the Mori–Tanaka method to elucidate the effective electromechanical properties. Subsequently, we describe the numerical homogenization techniques, specifically finite element analysis of a representative volume element (RVE), to validate and complement the analytical insights.

2.1. Constitutive equations

The constitutive equations to describe piezoelectric materials assuming linear static case without body charge or forces can be given in the following form,

$$\begin{aligned} \sigma_{ij} &= C^E_{ijkl}\varepsilon_{kl} - e_{kij}E_k, \\ D_i &= e_{ikl}\varepsilon_{kl} + \epsilon^{\varepsilon}_{ik}E_k. \end{aligned} \tag{1}$$

These equations correlate stresses (σ_{ij}), strains (ε_{kl}), electric field (E_k) and electrical displacements (D_i). In the expressions above, C^E_{ijkl} is the fourth-order elasticity tensor under constant electric field (i.e., short circuit boundary conditions), $\epsilon^{\varepsilon}_{ik}$ is the second-order free body electric tensor (under constant strain), and e_{kij} is the third-order piezoelectric strain coupling tensor. Taking into account the symmetry of the tensors σ_{ij}, ε_{ij}, C^E_{ijkl} and $\epsilon^{\varepsilon}_{ij}$, Eq. (1) can be written – by using Voigt's notation – in a vector/matrix notation as

$$\begin{bmatrix} \boldsymbol{\sigma} \\ \boldsymbol{D} \end{bmatrix} = \begin{bmatrix} \boldsymbol{C}^E & \boldsymbol{e}^T \\ \boldsymbol{e} & -\boldsymbol{\epsilon}^{\varepsilon} \end{bmatrix} \begin{bmatrix} \boldsymbol{\varepsilon} \\ -\boldsymbol{E} \end{bmatrix}. \tag{2}$$

where the superscript T denotes a transposed matrix.

Another widely used alternative and equivalent representation consists in writing the constitutive Eq. (2) in the following form:

$$\begin{bmatrix} \boldsymbol{\varepsilon} \\ \boldsymbol{D} \end{bmatrix} = \begin{bmatrix} \boldsymbol{S}^E & \boldsymbol{d}^T \\ \boldsymbol{d} & \boldsymbol{\epsilon}^{\sigma} \end{bmatrix} \begin{bmatrix} \boldsymbol{\sigma} \\ \boldsymbol{E} \end{bmatrix}, \tag{3}$$

where the compliance matrix under constant electric field $\boldsymbol{S}^E$, the piezoelectric stress coupling matrix $\boldsymbol{d}$ and the dielectric permittivity

matrix under constant stress $\boldsymbol{\epsilon}^{\sigma}$ hold the following relationships with the Eq. (2) constitutive matrix terms: $\mathbf{S}^{E} = \mathbf{C}^{E^{-1}}$, $\mathbf{d} = \mathbf{e}\,\mathbf{S}^{E}$ and $\boldsymbol{\epsilon}^{\sigma} = \boldsymbol{\epsilon}^{\epsilon} + \mathbf{d}\,\mathbf{e}^{T}$.

For the sake of compactness, the piezoelectric constitutive Eq. (2) can be further simplified as

$$\boldsymbol{\Sigma} = \boldsymbol{L}\boldsymbol{Z}, \tag{4}$$

where $\boldsymbol{\Sigma}$ and $\boldsymbol{Z}$ are the 9×1 column vectors (i.e., $\boldsymbol{\Sigma}^{T} = [\boldsymbol{\sigma}^{T}\ \boldsymbol{D}^{T}]$ and $\boldsymbol{Z}^{T} = [\boldsymbol{\epsilon}^{T}\ -\boldsymbol{E}^{T}]$) and $\boldsymbol{L}$ is the 9×9 matrix presented in Eq. (2).

2.2. Electromechanical properties via Mori–Tanaka model

The effective electromechanical properties of the composite can be evaluated by means of effective field method (EFM) as

$$\boldsymbol{L} = \boldsymbol{L}_{o} - c_{r}(\boldsymbol{L}_{r} - \boldsymbol{L}_{o})\boldsymbol{A}_{r}, \tag{5}$$

where c_r is the volume fraction of the active phase (i.e., the piezoelectric fibers -in 1-3-type composite- or the piezoelectric inclusions -in 0-3-type composite-), $\boldsymbol{L}_o$ and $\boldsymbol{L}_r$ describe the electromechanical properties of the matrix and the piezoelectric inclusions, respectively, and $\boldsymbol{A}_r$ is the strain-potential gradient concentration matrix of the active phase.

Several procedures exist for evaluating the concentration tensor. One of most widely used approached is the Mori–Tanaka (MT) scheme [37]. According to MT, $\boldsymbol{A}_r$ can be expressed as

$$\boldsymbol{A}_{r} = \boldsymbol{A}_{r}^{dil}\left(\ (1 - c_{r})\boldsymbol{I} + c_{r}\boldsymbol{A}_{r}^{dil}\ \right)^{-1} \tag{6}$$

where $\boldsymbol{A}_{r}^{dil} = (\boldsymbol{I} + \boldsymbol{S}\boldsymbol{L}_{o}^{-1}(\boldsymbol{L}_{r} - \boldsymbol{L}_{o})\ )^{-1}$, being $\boldsymbol{I}$ the identity matrix and $\boldsymbol{S}$ the coupled electroelastic Eshelby's matrix. The components of $\boldsymbol{S}$ depend on both, the properties of the matrix and the geometry of the inclusions. The explicit components of ($\boldsymbol{S}$) for a 1-3 connectivity scheme, with transversely isotropic cylindrical -piezoelectric- inclusions in a transversely isotropic -piezoelectric- matrix, can be found in [12]. However, when a 0-3 connectivity scheme is considered, the explicit expressions for the $\boldsymbol{S}$ terms can only be obtained in [13,38] for transversely isotropic spherical -piezoelectric- inclusions in an isotropic -dielectric- matrix. For a spherical inclusion in an anisotropic piezoelectric solid, the Eshelby's matrix components cannot be obtained analytically and should be computed numerically. The interested reader is referred to [39] for transversely isotropic piezoelectric composites with spherical inclusions and to [40] for orthotropic piezoelectric composites.

2.3. Electromechanical properties via RVE finite element modeling

Another approach to estimate the electromechanical properties of the piezoelectric composites is the finite element analysis of a RVE – or unit cell – of the material. It should be noted that the complete microstructure can be obtained by tessellation of this periodic unit cell. Due to this periodicity, the unit cell is taken as a RVE, which allows us to consistently obtain the macroscopic response of the piezocomposite (i.e., $\bar{\boldsymbol{\Sigma}} = \boldsymbol{L}^{\text{eff}}\,\bar{\boldsymbol{Z}}$). Since the piezoelectric composite materials can be represented as a periodic array of unit cell volumes, the periodic boundary conditions must be applied on the RVE models. Consequently, each RVE in the PE composite exhibits the same deformation mode, so there is no separation or overlap between the neighboring RVEs. Then, proper periodic boundary conditions should be considered in the numerical implementation.

The averaging process of the different parameters on a given material unit cell volume V can be approximated – using the FEM – by the weighted average over the RVE volume as

$$\bar{\boldsymbol{\Sigma}} = \frac{1}{V}\int_{V}\boldsymbol{\Sigma}\,dV \approx \frac{1}{V}\sum_{e=1}^{N_e}\boldsymbol{\Sigma}_{e}\,V_{e}, \qquad \bar{\boldsymbol{Z}} = \frac{1}{V}\int_{V}\boldsymbol{Z}\,dV \approx \frac{1}{V}\sum_{e=1}^{N_e}\boldsymbol{Z}_{e}\,V_{e}. \tag{7}$$

In the expressions above, N_e is the number of finite elements of the complete unit cell and V_e is the volume of the e-element.

The commercial software ANSYS APDL is used for numerical calculations in RVE finite element modeling. In Fig. 1 we can see the finite element meshes of the RVEs under: 1-3 type connectivity conditions - Fig. 1(a)- and 0-3 type connectivity conditions - Fig. 1(b)-, for an active phase volume fraction of 22.22%. To obtain the homogenized effective properties, we apply the macroscopic periodic boundary conditions to the RVE by coupling opposite nodes on opposite boundaries (i.e., S_j^+ and S_j^-) in the usual way:

$$u_i^{S_j^+} - u_i^{S_j^-} = \bar{\varepsilon}_{ij}\,(x_j^{S_j^+} - x_j^{S_j^-}), \qquad \phi^{S_j^+} - \phi^{S_j^-} = -\bar{E}_i\,(x_j^{S_j^+} - x_j^{S_j^-}), \tag{8}$$

where $\bar{\varepsilon}_{ij}$ is the average strains and $\bar{E}_i$ is the average electric field defined. In terms of modeling, this means that each node (S_j^+) has its displacements related to those of node on the opposite surface (S_j^-). A detailed explanation can be found in [7,17].

The calculation of the effective coefficient L_{mn}^{eff} has to apply the boundary conditions in the RVE in such a way that, except for $\bar{Z}_n$, all other mechanical strains and gradients of electric potential ($\bar{Z}_m$, being $m \neq n$) become zero. Then, the mean value of $\bar{\Sigma}_m$ is calculated according to Eq. (7). Therefore, the material parameters can be obtained from the relation average over the RVE volume as

$$L_{mn}^{\text{eff}} = \frac{\bar{\Sigma}_m}{\bar{Z}_n}. \tag{9}$$

where the subindex n corresponds to the applied strain/electrical field and the m corresponds to the average stress/electrical displacement computed in the RVE.

3. Lead-free piezocomposites performance

In this section, we present the effective material properties and some figures of merit for various combinations of lead-free piezocomposites and connectivities. For actuating and sensing applications, the piezoelectric strain constant (d_{ij}), or the piezoelectric voltage constant (e_{ij}), can be an appropriate criterion. Conversely, when evaluating piezoelectric materials for energy harvesting, energy conversion efficiency becomes more significant. In this context, the electromechanical coupling factor emerges as a key metric, particularly the thickness electromechanical coupling factor (k_t) and the planar coupling factor (k_p). They serve as crucial indicators in piezoelectric materials, delineating the efficiency with which an electrical stimulus can be transformed into mechanical response and vice versa, thus quantifying the bidirectional energy conversion capability. According to [41], these factors are quantitatively defined by

$$k_{t} = \left(\ 1 - \left(\frac{C_{33}^{E}}{C_{33}^{D}}\right)\ \right)^{1/2} \tag{10}$$

and

$$k_{p} = \left(\ 1 - \left(\frac{\epsilon_{33}^{\epsilon}}{\epsilon_{33}^{\sigma}}\right)\left(\frac{C_{33}^{D}}{C_{33}^{E}}\right)\ \right)^{1/2}, \tag{11}$$

respectively, where $C_{33}^{D} = C_{33}^{E} + e_{33}^{2}/\epsilon_{33}^{\epsilon}$. Physically, the factor k_t quantifies the coupling between the electric field and the mechanical strain in the direction of polarization (typically the thickness of a piezoelectric disk). A higher value of k_t implies a more efficient conversion between the electrical and mechanical energies in that specific direction. On the other hand, the factor k_p pertains to the in-plane coupling, or equivalently, the efficiency of energy conversion in the plane orthogonal to the polarization direction. Both of these factors, which range between 0 (no coupling) and 1 (perfect coupling), serve as tools in the selection and design of piezoelectric devices, ensuring optimal performance by maximizing the electromechanical energy conversion.

This section is divided into three subsections. Firstly, the accuracy of the computing frameworks implemented in this work to obtain the effective electromechanical properties of piezocomposite is validated

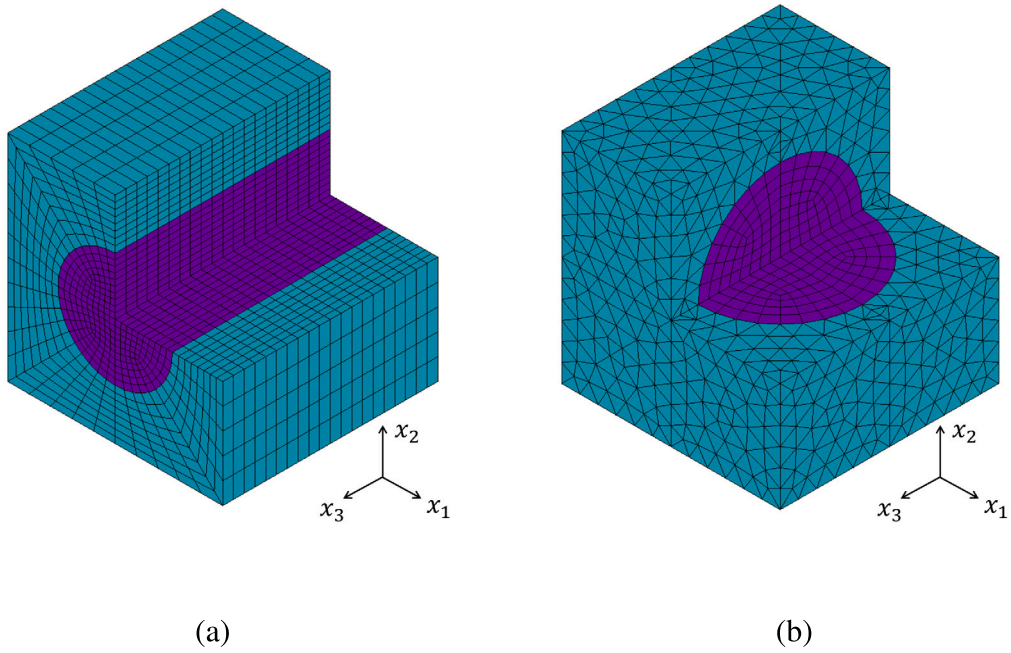

Fig. 1. Finite element meshes of the RVEs under: (a) 1-3 type connectivity conditions and (b) 0-3 type connectivity conditions. These meshes correspond to an active phase volume fraction of 22.22%. It should be noted that x_3-axis is the poling direction.

by comparison with some experimental results of a lead-based piezocomposite obtained from the literature. Secondly, through rigorous computational analysis, we quantify the performance metrics of the lead-free piezocomposites under these configurations, providing a clear comparative study with established lead PZT piezoelectrics to gauge the relative performance and potential advantages of the lead-free alternatives. Finally, the role of CNT polymeric matrix tuning in the BTO & PDMS lead-free piezocomposite is also analyzed.

3.1. Computing frameworks validation

To illustrate the accuracy of the computing frameworks implemented in this work to obtain the effective electromechanical properties of piezocomposites (i.e., the MT methodology and the RVE finite element modeling), we consider the PZT & Epoxy (Araldite D) piezoelectric composite in a 1-3 configuration, as experimentally studied in [11]. Figs. 2 (a-c) present the experimental and the computed variation of the relative dielectric constant $\epsilon^{\sigma}_{33}/\epsilon_o$ (being $\epsilon_0 = 8.85418 \cdot 10^{-12}$ F/m), the thickness electromechanical coupling factor k_t and the charge constant d_{33}, with the volume fraction of PZT-7A. We can see how the computed results present an excellent agreement with the experimental data. The computed results presented in Figs. 2 (a) and (b) were obtained for the PZT-7A properties given in Table 1 and Table 2, where x_3-axis is the poling direction. However, similar to [11], the calculated results for the effective charge constant d_{33} were obtained considering $d_{33} = 167 \cdot 10^{-12}$ m/V ($e_{33} = 12.28$ C/m^2) for the PZT-7A. It can be seen that the agreement is quite good. Therefore, the MT methodology and the RVE finite element modeling can be considered to study the performance of several piezoelectric composites.

3.2. Analysis of 0-3 and 1-3 configurations

Throughout this paper, we utilize the lead-based piezocomposite (PZT-7A & Epoxy) as a benchmark for all figures of merit. First, we are going to analyze the mechanical performance of the lead-free piezocomposite in comparison to our established benchmark. Figs. 3 (a-c) present the effective elastic coefficients ($C^E_{11}, C^E_{13}, C^E_{33}$), respectively, for different piezocomposites (i.e., PZT-7A & Epoxy, BTO & PDMS, BTO & PVDF and KNNS-BNZH & Polyethylene) and different configurations (i.e., 1-3 and 0-3 configurations), as a function of the active phase volume fraction. We can observe that, firstly, the higher mechanical performance is obtained for the lead-based piezocomposite (PZT-7A & Epoxy). The lead-free 0-3 piezocomposites could be ordered in terms of increasing C^E_{11}, C^E_{13} and C^E_{33} elastic coefficients performance as: BTO & PDMS less than KNNS-BNZH & Polyethylene less than BTO & PVDF. However, it cannot be like this for the lead-free 1-3 piezocomposites. When 1-3 configuration is adopted, they can only be ordered in that way when C^E_{11} elastic coefficient performance is observed. Their C^E_{33} elastic coefficient values are quite similar, and, for C^E_{13} elastic coefficient, the lead-free piezocomposites ranking is a function of the active phase volume fraction. Secondly, for all the piezoelectric composites, the values of these coefficients increase with the active phase volume fraction, being the higher increments of the elastic coefficients observed for the PZT-7A & Epoxy and the BTO & PVDF piezocomposites. However, for the C^E_{33} coefficient, these increments are clearly affected by the piezoelectric configurations. Since the 1-3 configuration presents a clear orientation of the active phase in the x_3-direction (see Fig. 1(a)), the slope of the C^E_{33}-active phase volume fraction curve is significantly greater in the 1-3 configuration than in the 0-3 configuration – for all the piezocomposites –.

In Fig. 4, the variation of piezoelectric strain coefficients against the volume fraction of the active phase is elucidated for different composite systems. The composites encompass dielectric matrices, including epoxy (Araldite D), PDMS, and polyethylene. Additionally, the piezoelectric matrix (indicated in all figures afterhere by dashed lines), PVDF, is scrutinized for comparison. It is evident that for the dielectric matrices, the effective piezoelectric coupling approaches zero in the absence of active phases. In contrast, for the piezoelectric PVDF matrix, a non-zero effective coupling remains, as expected. In Fig. 4(a), the cross e_{31} coefficients for both the 1-3 and 0-3 configurations are illustrated. As the volume fraction of the active phase is increased, an enhancement in effective coupling is discernible for composites with dielectric matrices. On the contrary, for the piezoelectric matrix, an intriguing interplay of the piezoelectric components is observed, leading to a scenario in which the cross coefficient attenuates to zero for some volume fraction within the range from 0.4 to 0.5. Among the various

Table 1
Material properties of the piezoelectric constituents of the piezocomposites.

Material	PZT-7 [11]	BTO [35]	PVDF [16]	KNNS-BNZH [36]
Elastic coefficients (Pa)				
$C_{11}^E(10^{10})$	14.8	27.51	0.38	13.62
$C_{12}^E(10^{10})$	7.62	17.89	0.19	8.62
$C_{13}^E(10^{10})$	7.42	15.155	0.10	6.59
$C_{22}^E(10^{10})$	14.8	27.51	0.32	13.62
$C_{23}^E(10^{10})$	7.42	15.155	0.09	6.59
$C_{33}^E(10^{10})$	13.1	16.48	0.12	9.85
$C_{44}^E(10^{10})$	2.54	5.43	0.07	2.28
$C_{55}^E(10^{10})$	2.54	5.43	0.09	2.28
$C_{66}^E(10^{10})$	3.59	11.31	0.09	2.50
Piezoelectric coefficients (C/m^2)				
e_{31}	−2.1	−2.69	0.024	−11.2
e_{32}	−2.1	−2.69	0.001	−11.2
e_{33}	9.5	3.65	−0.027	15.9
e_{15}	9.2	21.3	0	15.6
Relative permittivity				
$\epsilon_{11}^{\epsilon}/\epsilon_0$	460	1970	7.4	1100
$\epsilon_{22}^{\epsilon}/\epsilon_0$	460	1970	9.3	1100
$\epsilon_{33}^{\epsilon}/\epsilon_0$	235	109	7.6	975

Table 2
Material properties of the dielectric constituents of the piezocomposites.

Material	Araldite D [11]	PDMS [42]	Polyethylene [20]
Elastic coefficients (Pa)			
$C_{11}^E(10^{10})$	0.8	0.03342	0.0778
$C_{12}^E(10^{10})$	0.44	0.03329	0.0195
$C_{13}^E(10^{10})$	0.44	0.03329	0.0195
$C_{33}^E(10^{10})$	0.8	0.03342	0.0778
$C_{44}^E(10^{10})$	0.18	0.00006671	0.0292
$C_{66}^E(10^{10})$	0.18	0.00006671	0.0292
Relative permittivity			
$\epsilon_{11}^{\epsilon}/\epsilon_0$	4.2	2.72	2.3
$\epsilon_{33}^{\epsilon}/\epsilon_0$	4.2	2.72	2.3

systems evaluated, the PZT-7 A & Epoxy composite exhibits the most pronounced increase in the piezoelectric response. Additionally, the 1-3 configuration of the KNNS-BNZH & Polyethylene system manifests a significant improvement, underscoring its potential efficacy for this pattern connectivity. In Fig. 4(b), the variation of the e_{33} coefficient is depicted. For the 1-3 configuration, all evaluated systems demonstrate a significant amplification, with the KNNS-BNZH & Polyethylene composite capturing attention due to its pronounced enhancement. In the context of the 0-3 configuration, once again a piezoelectric interplay between the matrix and additive particles emerges for the BTO & PVDF composite; resulting in a null effective coupling around a volume fraction of 0.35. Of all the systems under this configuration, the PZT-7 A & Epoxy composite evinces the most substantial advancement.

Fig. 5 shows the evolution of the piezoelectric stress coefficients with the volume fraction of the active phase for the studied composite systems. Fig. 5 (a) presents the behavior of the cross components d_{31}. In parallel to our discourse on effective piezoelectric strain coefficients, the first observation is that, for the dielectric matrices, the effective piezoelectric coupling essentially attenuates to nullity in the absence of the active phases. On the contrary, with the piezoelectric PVDF matrix, the system retains a substantial effective coupling underscoring the intrinsic piezoelectric nature of the PVDF matrix. Also, a similar piezoelectric interplay is observed for the BTO & PVDF system, where d_{31} decreases with the addition of the active phase. However, no null effective coupling is observed for 0-3 configuration. In contrast, we observe that for the 1-3 configuration, a null effective coupling occurs at a notably low volume fraction (≈ 0.02) and rapidly the coefficient increases until a volume fraction of approximately 0.1, and then monotonically increases with a lower gradient. Upon the incorporation of BTO, the effective d_{31} manifests an augmentation exceeding fourfold the intrinsic value of the matrix, albeit accompanied by an inversion in polarity. This behavior can also be observed for the d_{33} component, as depicted in Fig. 5 (b). Interestingly, for the 1-3 configuration, even a minimal addition of BTO to the PDMS matrix results in nearly invariant effective piezoelectric coefficients d_{31} and d_{33} across the entire volume fraction spectrum. Another noteworthy mention is the 1-3 configuration for the KNNS-BNZH & Polyethylene system, which shows a notable performance, suggesting its potential for eco-friendly applications with this connectivity pattern. Within this comparative exploration, the PZT-7 A & Epoxy and BTO & PDMS composite stands out among the dielectric matrix systems, showcasing the most prominent boost in its piezoelectric response for configurations 0-3.

The relative dielectric permittivity coefficients, $\epsilon_{11}^{\sigma}/\epsilon_0$ and $\epsilon_{33}^{\sigma}/\epsilon_0$, as functions of the active phase volume fraction are illustrated in Fig. 6. Subplot (a), delineating the behavior of ϵ_{11}, consistently reveals a trend: permittivity increases with the volume fraction. The curves representing each composite system are smooth and largely parallel. Among them, the BTO & PVDF composite system stands out, consistently registering the highest permittivity values and setting a benchmark for the others. This is followed by the PZT-7 A & Epoxy composite. Meanwhile, the BTO & PDMS and KNNS-BNZH & Polyethylene composites display more moderate trajectories.

In Fig. 6(b), focusing on the ϵ_{33}^{σ} permittivity, similar trends are observed for the 0-3 configuration. Specifically, the BTO & PVDF composite maintains its dominance. However, in the 1-3 configuration, the nonlinear behavior becomes more pronounced. The relative dielectric permittivities for BTO & PDMS and BTO & PVDF converge at volume fractions close to 0.1. As a global observation, all systems exhibit an increase in permittivity as the volume fraction increases, albeit at different rates and magnitudes. Notably, for this 1-3 configuration, the

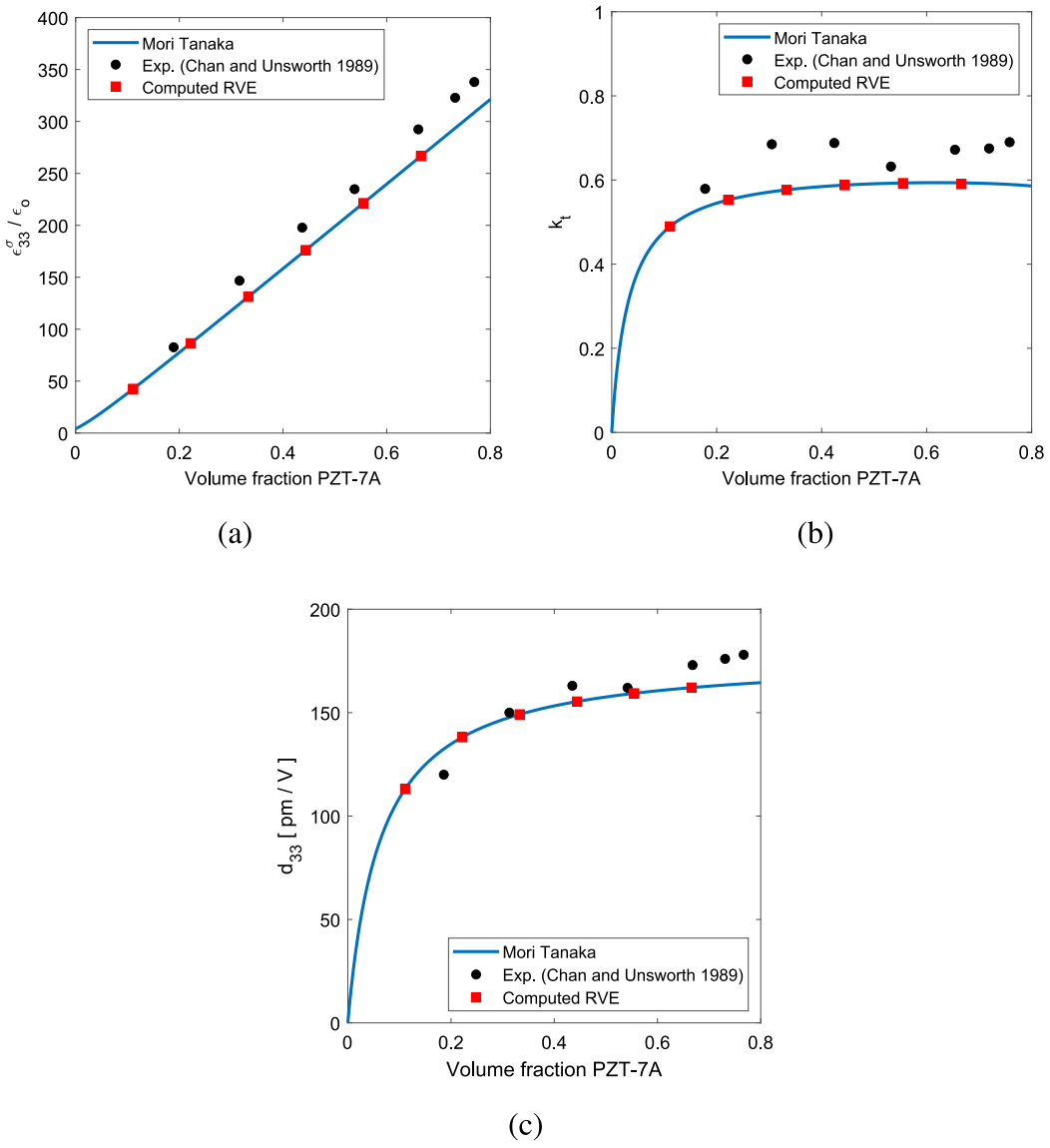

Fig. 2. Experimental and computed variation of the: (a) relative dielectric constant $\epsilon^{\sigma}_{33}/\epsilon_o$, (b) thickness coupling constant k_t and (c) charge constant d_{33}, with volume fraction of PZT-7A.

KNNS-BNZH & Polyethylene composite presents the highest permittivity values across nearly the entire volume fraction spectrum. The observation of these significant values for the permittivity ϵ^{σ}_{33} leads us to examine the influence of the permittivity on piezoelectric performance, especially in the context of energy harvesting applications. The literature suggests that lower permittivity is generally preferred, as it is crucial in enhancing both the sensitivity and the harvesting figure of merit [43,44]. This assertion is further supported in our study by examining the figure of merit k_t as defined in Eq. (10). For illustrative purposes, we assume constant elasticity. The relationship between k_t, the piezoelectric e_{33} coefficient, and the dielectric coefficient $\epsilon^{\varepsilon}_{33}$ is depicted in Fig. 7. The graphical representation clearly illustrates that lower values of $\epsilon^{\varepsilon}_{33}$ correspond to a more favorable k_t factor, particularly at reduced values of e_{33}. Consequently, our analysis aligns with the broader consensus in the field that for enhanced energy conversion performance, a lower value of $\epsilon^{\varepsilon}_{33}$ proves to be more advantageous. This leads to the conclusion that the high permittivity values observed in Fig. 6(b) are not optimal for energy conversion efficiency in piezoelectric applications, highlighting the need for careful account this effect when designing microstructural features in piezoelectric composites for such purposes.

Figs. 8 (a) and (b) show the k_t and k_p electromechanical factors, respectively. In the 1-3 configuration, k_t increases rapidly from its initial value and subsequently reaches a plateau at distinct levels. In particular, the pure dielectric matrices take null value for k_t as derived from Eq. (10). Both the KNNS-BNZH & Polyethylene and PZT-7 A & Epoxy systems converge at an identical saturation point. However, systems incorporating BTO to the matrix stabilize at slightly diminished levels compared to the previous two. In the 1-3 configuration, the planar electromechanical coupling factor k_p demonstrates discernible peaks at relatively lower volume fractions. In particular, the PZT-7 A & Epoxy system maintains a consistently elevated value of k_p across the entire volume fraction spectrum, while the BTO & PDMS system exhibits a pronounced peak, surpassing the other composites at its peak. Both the BTO & PVDF and KNNS-BNZH & Polyethylene systems also exhibit peaks, though at different volume fractions and magnitudes. Identifying these peaks is of paramount importance within the context of material optimization. For the 0-3 configuration, both electromechanical factors exhibit similar behavior. Specifically, the largest factors are observed for the pure piezoelectric matrix of PVDF. These factors diminish with the introduction of BTO particles but remain higher up to volume fractions of about 0.3. Beyond this volume

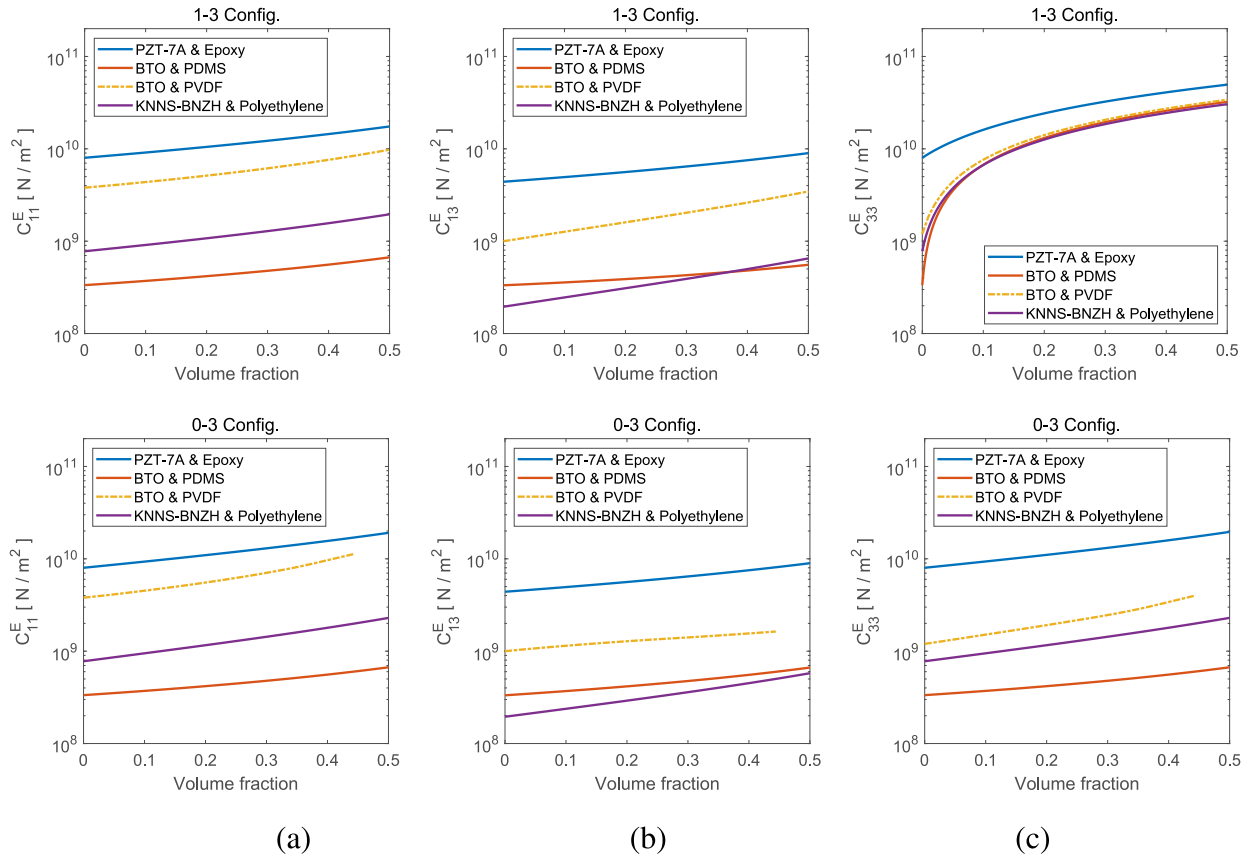

Fig. 3. Effective elastic coefficients: (a) C_{11}^E, (b) C_{13}^E and (c) C_{33}^E, for different piezoelectric composites (i.e., PZT-7A & Epoxy, BTO & PDMS, BTO & PVDF and KNNS-BNZH & Polyethylene) and different configurations (i.e., 1-3 and 0-3 configurations), as a function of the active phase volume fraction.

Table 3
Electroelastic constants of PDMS matrix doped with CNT from Cañamero et al. [7].

CNT Volume fraction ($f_{_{CNT}}$)	0.0%	0.061%	0.304%	0.504%	0.544%	0.582%	0.602%
f_{CNT}/f_c	0.0	0.10	0.50	0.82	0.89	0.95	0.99
Elastic coefficients (GPa)							
C_{11}^E	0.3342	0.5058	1.196	1.762	1.876	1.984	2.044
C_{12}^E	0.3329	0.3894	0.6218	0.8092	0.8472	0.8833	0.9055
C_{13}^E	0.3329	0.3894	0.6218	0.8092	0.8472	0.8833	0.9055
C_{33}^E	0.3342	0.5058	1.196	1.762	1.876	1.984	2.044
C_{44}^E	$6.671 \cdot 10^{-4}$	0.05819	0.2873	0.4765	0.5144	0.5505	0.5692
C_{66}^E	$6.671 \cdot 10^{-4}$	0.05819	0.2873	0.4765	0.5144	0.5505	0.5692
Relative permittivity							
$\epsilon_{11}^{\epsilon}/\epsilon_o$	2.72	3.09	6.25	22.64	40.54	119.48	694.18
$\epsilon_{33}^{\epsilon}/\epsilon_o$	2.72	3.09	6.25	22.64	40.54	119.48	694.18

fraction, the PZT-7 A & Epoxy system possesses the highest electromechanical coupling factors. For systems with a dielectric matrix, the factors increase upon the addition of the active phases. Among them, the PZT-7 A & Epoxy composite system outperforms, followed by the KNNS-BNZH & Polyethylene, and lastly, the BTO & PDMS system.

3.3. CNT tuned matrix in piezocomposites

The enrichment of matrices with nanoadditives to tune and augment the properties of piezocomposites has garnered increasing attention in the realm of advanced materials research. In this section, we delve into the intricacies of CNT incorporation within the matrices, elucidating its implications on the effective mechanical and electromechanical characteristics of the lead-free piezocomposites. By comprehending the role of CNTs as tuning agents, we aim to underscore the potential of these nanostructures in paving the way for next-generation piezocomposite materials. For this purpose, the BTO & PDMS system is considered, where the PDMS matrix is doped with CNTs. The electroelastic constants of the PDMS matrix doped with CNT are taken from Cañamero et al. [7], and summarized in Table 3. The addition of MWCNTs also increases the dielectric permittivity of the matrix. Based on existing experimental evidence [45,46], the variation of the dielectric constant

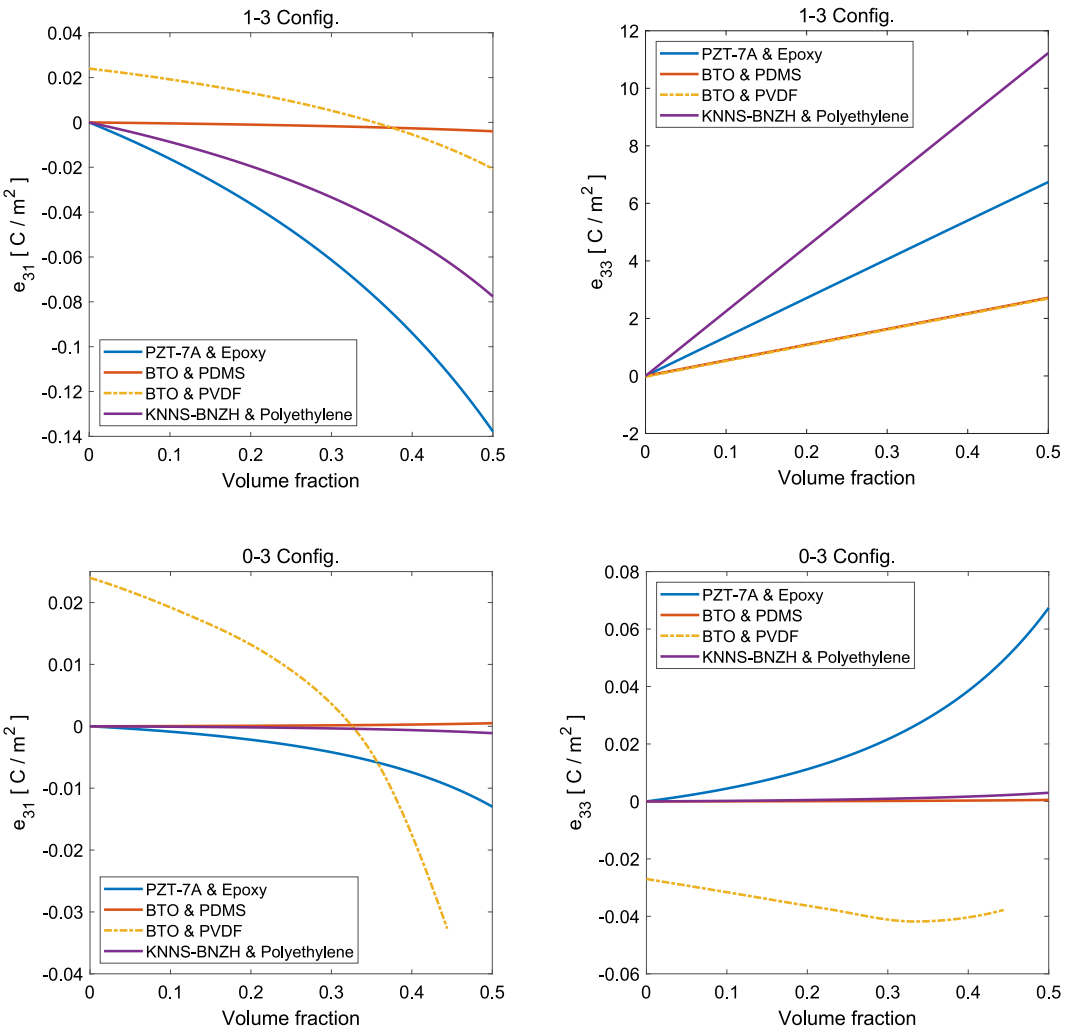

Fig. 4. Evolution of the piezoelectric strain coefficients with the volume fraction of the active phase. (a) Components e_{31} for 1-3 and 0-3 configurations. (b) Components e_{33} for 1-3 and 0-3 configurations.

with f_{CNT} follows a percolation behavior, described by a power-law

$$\epsilon_m^{\varepsilon\,*} = \epsilon_m^{\varepsilon}\left(\frac{f_c}{f_c - f_{CNT}}\right)^{p}, \tag{12}$$

where ϵ_m^{ε} is the relative permittivity of the pristine polymer matrix, f_c is the percolation threshold of the nanotubes, f_{CNT} is the volume fraction of the nanotubes in the PDMS matrix, and p is a critical exponent determining the percolative variation of the effective permittivity. In this work, parameter p is set to 1.2 for PDMS polymer. The percolation threshold, f_c, and the critical exponent, p, are functions of mainly the aspect ratio of the MWCNTs and the agglomeration characteristics. This was discussed in detail by authors [7].

Note that our study primarily focuses on modifying the dielectric properties of piezocomposites, particularly within the PDMS matrix, through the incorporation of CNTs. The proposed approach follows the phenomenological model based on percolation theory, as delineated by Eq. (12), and is grounded by experimental data. We recognize that the significant contrast in conductivity between CNTs and the matrix may lead to the formation of nanocapacitors – a phenomenon referred to as Maxwell-Wagner-Sillars polarization – which could consequently influence the dielectric properties. Although these interfacial effects are not explicitly encompassed within our current model framework, they could exert a considerable influence on the effective dielectric properties of the matrix under specific conditions. Nonetheless, our model indirectly accounts for this nanocapacitor effect, among potential others, through the selection of parameters in the model given by Eq. (12). In other words, the described phenomenon is implicitly accounted for in our approach.

In Fig. 9, we can see the effective elastic coefficients of BTO & PDMS piezocomposite: (a) C_{11}^E, (b) C_{13}^E and (c) C_{33}^E, for different pattern connectivities (i.e., 1-3 and 0-3 configurations), as a function of the BTO volume fraction, and the CNT volume fraction relative to the percolation threshold (f_{CNT}/f_c). For all cases, we observe an increase in the elasticities as the CNT content approaches the percolation threshold. Same behavior is observed in Fig. 10 for the piezoelectric strain constants when a tunned matrix is considered. In Fig. 10(a) a substantial increase of the e_{31} component is observed for both pattern connectivities, but mainly remarkable for 0-3 configurations. The larger coefficients are obtained when the CNT content approaches the percolation threshold for all BTO volume fractions. Similar behavior is obtained for the e_{33} component when the 0-3 configuration is considered, however, the effect of CNT content is negligible for the 1-3 configuration (see Fig. 10(b)).

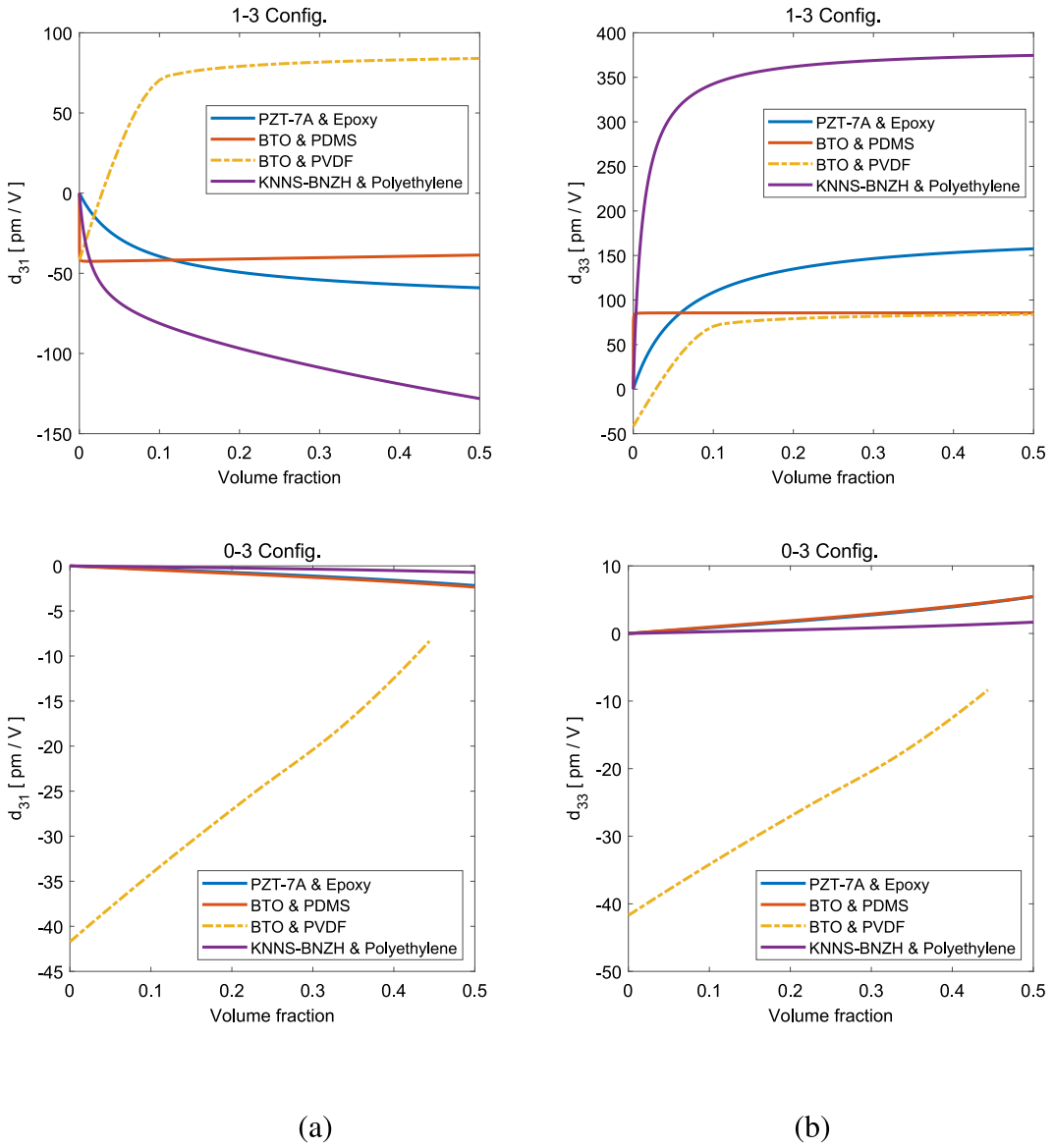

Fig. 5. Evolution of the piezoelectric stress coefficients with the volume fraction of the active phase. (a) Components d_{31} for 1-3 and 0-3 configurations. (b) Components d_{33} for 1-3 and 0-3 configurations.

The effective piezoelectric stress coefficients of the BTO & PDMS piezocomposite are depicted in Fig. 11. For the 1-3 configuration, there is a marked degradation in the d_{31} and d_{33} coefficients upon CNT addition. On the contrary, the 0-3 configuration sees a pronounced enhancement in these properties. As the CNT content approaches the percolation threshold, the improvement amplifies non-linearly, as illustrated in Fig. 11.

Fig. 12 illustrates the relative dielectric permittivities, $\epsilon^{\sigma}_{11}/\epsilon_0$ and $\epsilon^{\sigma}_{33}/\epsilon_0$, for different pattern connectivities. In subplot (a), the behavior of ϵ^{σ}_{11} is nearly linear with respect to the BTO volume fraction. Curves for varying the CNT content remain parallel to each other. However, as the CNT content approaches the percolation threshold, there is a noticeable enhancement in the relative constant $\epsilon^{\sigma}_{11}/\epsilon_0$. Subplot (b) presents a distinctly nonlinear trend for the dielectric constant ϵ^{σ}_{33} in the 1-3 configuration. The dielectric constant intensifies with increasing CNT enrichment. Interestingly, as the CNT content approaches the percolation threshold, ϵ^{σ}_{33} shows a declining trend with the volume fraction of the BTO. Particularly, at $f_{\mathrm{CNT}} \approx 0.95 f_c$, the curve slope transitions to zero for both configurations. Beyond this point, the slope assumes a negative value, as can be discerned from Fig. 12(b).

In Fig. 13(a), the electromechanical (thickness) coupling factor k_t is plotted against the BTO volume fraction. For both pattern configurations, an increase in k_t is observed with a higher BTO volume fraction, with this trend being more noticeable for the 1-3 configuration. For this connectivity, undoped matrices yield the highest coupling values, which are achieved even with minimal BTO presence, and then stabilize over the entire BTO volume fraction range. Introducing doping results in a reduction of the electromechanical coupling. In the 0-3 configuration, there is a consistent rise in coupling with BTO addition. Notably, the maximum coupling is found for a volume fraction slightly less than percolation, specifically with the curve of $f_{\mathrm{CNT}} = 0.95 f_c$, after which there is a decrement in performance for values approaching the percolation threshold at 0.99. In Fig. 13(b) concerning the 1-3 configuration, the planar electromechanical coupling factor k_p is presented as a function of the BTO volume fraction. The pure BTO & PDMS sample reveals a pronounced enhancement in k_p with the incremental addition of BTO, reaching a peak and then experiencing a minor diminishment. The influence of CNTs, characterized by different fractions (f_{CNT}), exhibits a diverse range of behaviors. The prominence of the peak diminishes with the inclusion of CNT into the matrix,

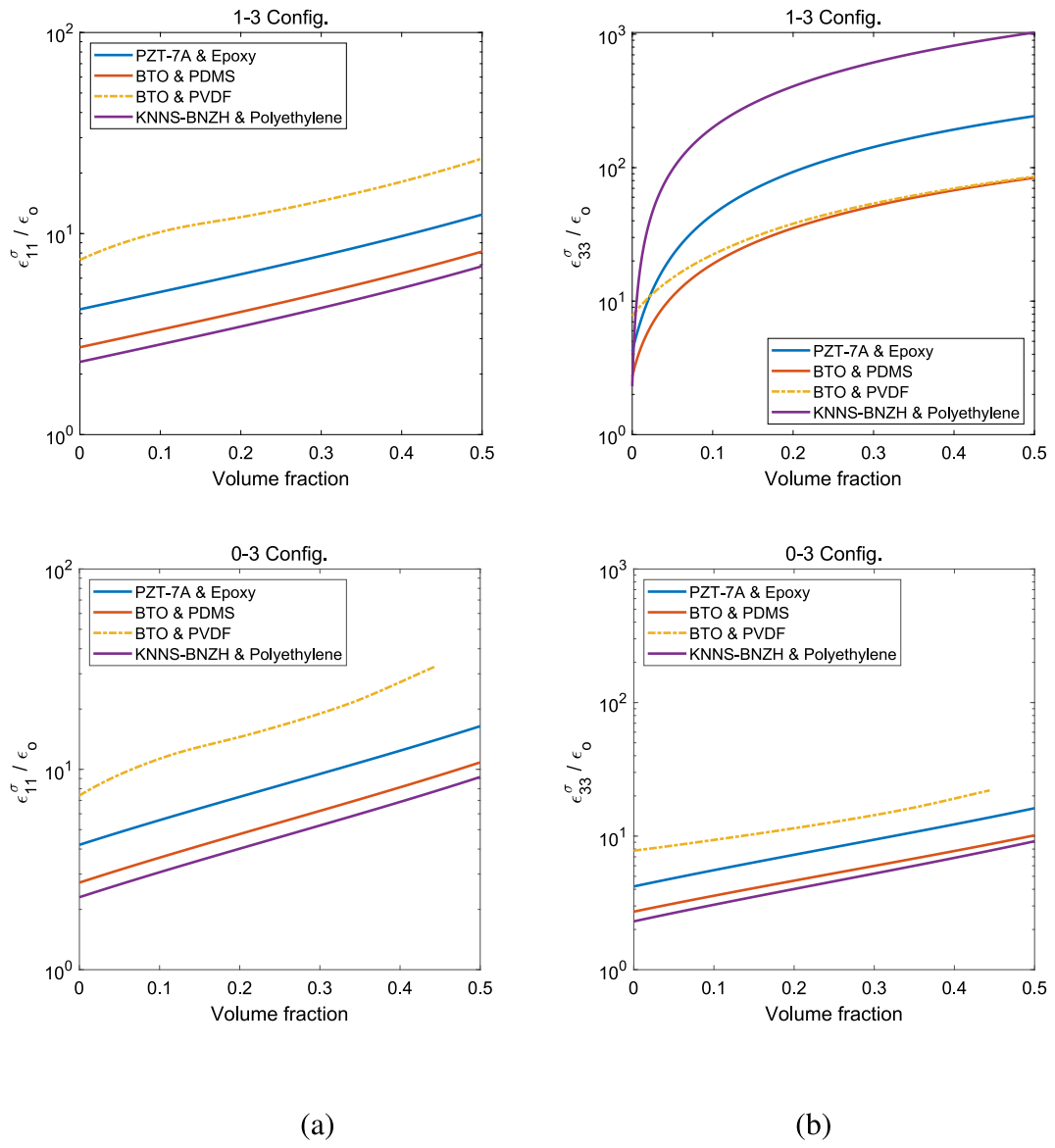

Fig. 6. Evolution of the relative dielectric permittivity coefficients with the volume fraction of the active phase. (a) Components $\epsilon_{11}^{\sigma}/\epsilon_0$ for 1-3 and 0-3 configurations. (b) Components $\epsilon_{33}^{\sigma}/\epsilon_0$ for 1-3 and 0-3 configurations.

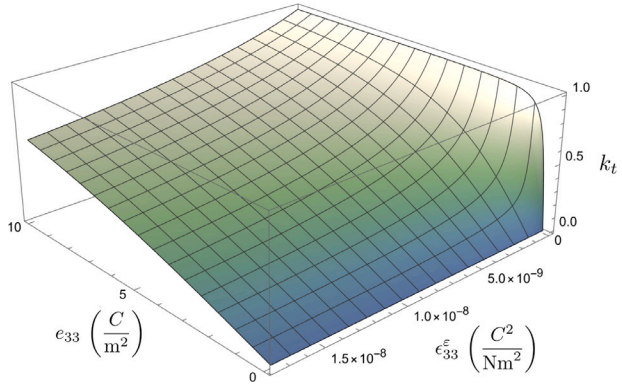

Fig. 7. Dependence of the k_t coefficient on $\epsilon_{33}^{\varepsilon}$. The lower the value of $\epsilon_{33}^{\varepsilon}$ is, the more favorable k_t factor is obtained, especially at low values of the e_{33} piezoelectric coefficient. The elasticity C_{33}^{E} is arbitrarily set to 10 GPa.

and this peak is manifest at elevated BTO volume fractions. The peak vanishes when f_{CNT}/f_c approaches approximately 0.8. Subsequent to this, the behavior of k_p is characterized by a consistent increase with the addition of BTO, tapering off as the matrix nears the percolation threshold. The behavior for the 0-3 configurations is similar to the described for k_t. Consequently, the value of f_{CNT} which optimize the electromechanical coupling coefficient k_p in 1-3 configuration depends on the active phase (i.e., BTO) volume fraction.

4. Conclusions

This work presents a comprehensive analysis of the performance of several lead-free piezoelectric composites, including BTO & PDMS, BTO & PVDF, and KNNS-BNZH & Polyethylene systems, in 1-3 and 0-3 connectivity patterns. We meticulously evaluated their effective properties and various FOMs, as functions of the active phase volume fraction. These were then compared with the performance of traditional lead-based counterparts, specifically PZT-7 A & Epoxy, across a range of applications including actuating, sensing, and energy harvesting.

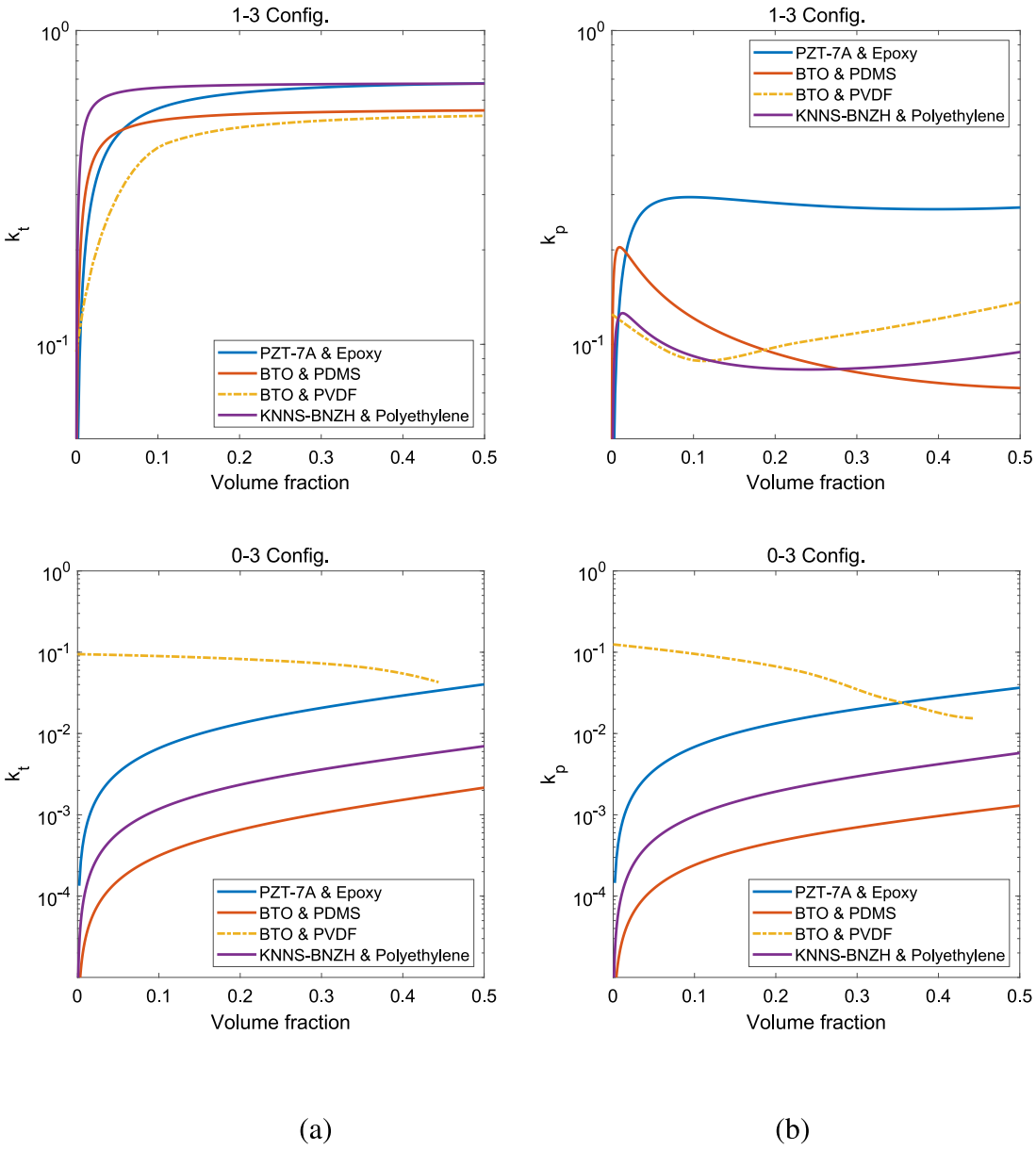

Fig. 8. Evolution of the electromechanical coupling factors with the volume fraction of the active phase. (a) The thickness electromechanical coupling factor k_t for 1-3 and 0-3 configurations. (b) The planar electromechanical coupling factor k_p for 1-3 and 0-3 configurations.

In summary, our numerical analyses provide substantial evidence that under certain connectivity patterns and active phase volume fractions, some of these lead-free composite systems can perform comparably or even superiorly to conventional lead-based piezocomposites. The results obtained notably reveal that:

- Observing the effective elastic coefficients (C_{11}^E, C_{13}^E and C_{33}^E), we first can observe that the lead-based piezocomposite presents higher mechanical performance (i.e., higher values of the elastic coefficients) in both connectivity patterns. Additionally, if we compare the lead-free piezocomposites, they can be ranked from low to high as: BTO & PDMS, KNNS-BNZH & Polyethylene and BTO & PVDF, for all the elastic coefficients, when 0-3 pattern is considered. Also for 1-3 connectivity patters, when C_{11}^E elastic coefficient is considered. For C_{33}^E elastic coefficient and 1-3 configuration, the lead-free piezocomposites present very similar values.
- The effective piezoelectric coefficients e_{31} and e_{33}, for both the 1-3 and 0-3 configurations, increase their values with the active phase volume fraction. In general, the PZT-7 A & Epoxy composite exhibits the most pronounced increase in the piezoelectric response. Additionally, the 1-3 configuration of the KNNS-BNZH & Polyethylene system manifests a significant improvement, underscoring its potential efficacy for this pattern connectivity. It is also interesting to mention that, for BTO & PVDF, in general, e_{31} coefficient does not improve with the addition of BTO. It depends on the value of the BTO volume fraction.
- This study has demonstrated that the effective piezoelectric stress coefficients, in general, are significantly influenced by the volume fraction of the active phase in the composites. As expected, the PVDF matrix maintains effective piezoelectric coupling even without the active phase, underscoring its inherent piezoelectric properties. In the 1-3 configuration, we observe a null effective coupling at a remarkably low volume fraction, which rapidly

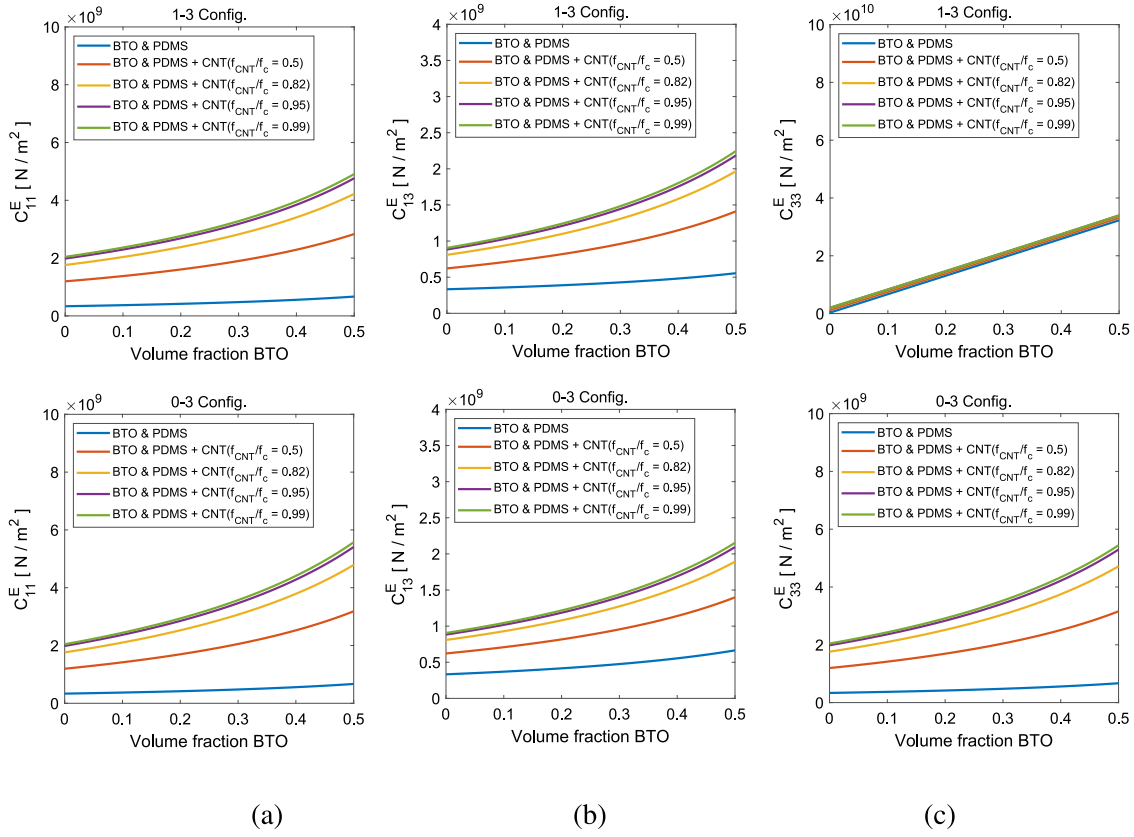

Fig. 9. Effective elastic coefficients of BTO & PDMS piezocomposite: (a) C_{11}^E, (b) C_{13}^E and (c) C_{33}^E, for different configurations (i.e., 1-3 and 0-3 configurations), as a function of the BTO volume fraction and the CNT volume fraction relative to the percolation threshold (f_{CNT}/f_c).

increases up to approximately 0.1, thereafter ascending more gradually. The inversion of polarity noted for the PVDF matrix with the addition of BTO, alongside the nearly constant effective coefficients in the BTO-PDMS matrix, are notable outcomes that provide valuable insights for the design of piezocomposite materials. Furthermore, the superior performance of the KNNS-BNZH & Polyethylene system in the 1-3 configuration indicates its promise for actuation applications. In the 0-3 configuration, the BTO & PVDF system exhibits optimal performance, which decreases as the BTO volume fraction increases.

- Analysis of the relative dielectric permittivity coefficients, $\epsilon_{11}^{\sigma}/\epsilon_0$ and $\epsilon_{33}^{\sigma}/\epsilon_0$, as functions of the active phase volume fraction has revealed distinct trends across the composite systems studied. The results for ϵ_{11}^{σ} indicates that permittivity increases with the volume fraction, with all systems exhibiting smooth and largely parallel trajectories. Notably, the BTO & PVDF composite system consistently registers the highest permittivity values, outperforming the others and establishing a benchmark within the group. Results also show that this trend persists for the ϵ_{33}^{σ} permittivity in the 0-3 configuration, with the BTO & PVDF composite maintaining its lead. However, in the 1-3 configuration, a more pronounced nonlinear behavior is observed. Here, the KNNS-BNZH & Polyethylene composite stands out, demonstrating the highest permittivity values across almost the entire volume fraction spectrum. Overall, an increase in permittivity with volume fraction is a common characteristic among the systems, although the rates and magnitudes of this increase vary.
- The thickness electromechanical coupling factor k_t increases with the active phase volume fraction, in 1-3 and 0-3 configuration, for all the piezoelectric composites considered but BTO & PVDF. However, it reaches the largest factors – compared to the rest of the other piezocomposites – for the pure piezoelectric matrix of PVDF. For the 1-3 pattern, k_t in all of the considered piezocomposites increases rapidly with the active phase volume fraction from its initial value and subsequently reaches a plateau at distinct levels. The highs values were obtained by the KNNS-BNZH & Polyethylene lead-free composite.
- The planar electromechanical coupling factor k_p presents a similar behavior of k_t when a 0-3 configuration is considered. However, for a 1-3 pattern, k_p shows discernible peaks in the three lead-free piezocomposites considered at relatively lower volume fractions. Nevertheless the PZT-7 A & Epoxy system maintains a consistently elevated value of k_p across the entire volume fraction spectrum. The BTO & PDMS system exhibits the highest peak. Both the BTO & PVDF and KNNS-BNZH & Polyethylene systems also exhibit peaks, though at different volume fractions and magnitudes. Identifying these peaks is of paramount importance within the context of material optimization.
- The role of the addition of CNTs in the polymeric matrix is also analyzed in the BTO & PDMS lead-free piezocomposite. The presence of CNTs in the PDMS matrix improves – for both patterns – the performance of mechanical coefficients (C_{11}^E, C_{13}^E, C_{33}^E), piezoelectric coefficients (e_{31}, e_{33}) and the dielectric coefficients (ϵ_{11}^{σ}, ϵ_{33}^{σ}). However, we have observed that the value of f_{CNT} which optimize their values is not the same in all these coefficients, and a negligible improvement in C_{33}^E and e_{33} coefficients.
- Piezoelectric coefficients (d_{31}, d_{33}) increase their values with the addition of CNTs when a 0-3 configuration is considered. However, their values decrease with f_{CNT} for 1-3 piezocomposite pattern.
- Finally, regarding the influence of f_{CNT} in the electromechanical coupling coefficients k_t and k_p, we have observed that, for 1-3 paterns, the addition of CNTs in the PDMS matrix reduces k_t coefficient, whereas increases k_p coefficient. Nevertheless, for

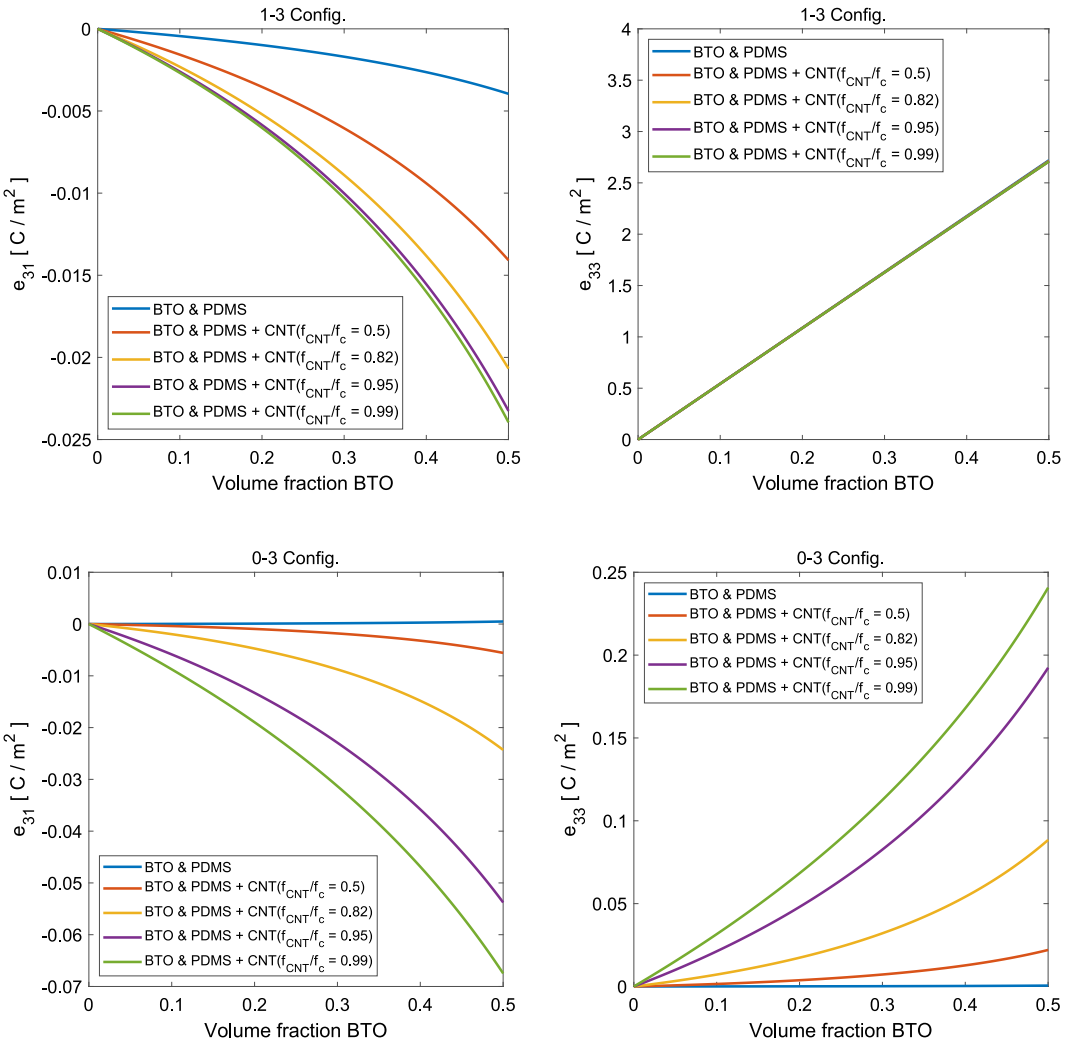

Fig. 10. Effective piezoelectric strain coefficients of BTO & PDMS piezocomposite: (a) e_{31} and (b) e_{33}, for different configurations (i.e., 1-3 and 0-3 configurations), as a function of the BTO volume fraction and the CNT volume fraction relative to the percolation threshold (f_{CNT}/f_c).

0-3 configurations, the addition of CNTs increases significantly both: k_t and k_p values. However, we have observed that the value of f_{CNT} which optimize these electromechanical coupling coefficients depends on the BTO volume fraction.

Therefore, this study not only reinforces the viability of lead-free piezoelectric composites in matching or surpassing the performance of traditional lead-based materials in certain configurations, but also highlights the critical role of connectivity patterns, active phase volume fraction, and strategic integration of CNTs in tailoring their electromechanical properties for specific application needs, thus marking a significant improvement in the pursuit of environmentally sustainable and high performance piezoelectric materials.

CRediT authorship contribution statement

Francisco J. Cañamero: Writing – original draft, Validation, Software, Methodology, Investigation, Formal analysis. **Federico C. Buroni:** Writing – review & editing, Writing – original draft, Supervision, Project administration, Investigation, Funding acquisition. **Luis Rodríguez-Tembleque:** Writing – review & editing, Writing – original draft, Supervision, Software, Project administration, Methodology, Investigation, Funding acquisition, Conceptualization.

Declaration of competing interest

The authors declare that they have no known competing financial interests or personal relationships that could have appeared to influence the work reported in this paper.

Data availability

Data will be made available on request.

Acknowledgments

This work was supported by the Ministerio de Ciencia e Innovación (Spain) . This publication is part of the R+D+i project, PID2022-137903OB-I00, funded by MICIU/AEI/10.13039/501100011033/ and by FEDER, EU.

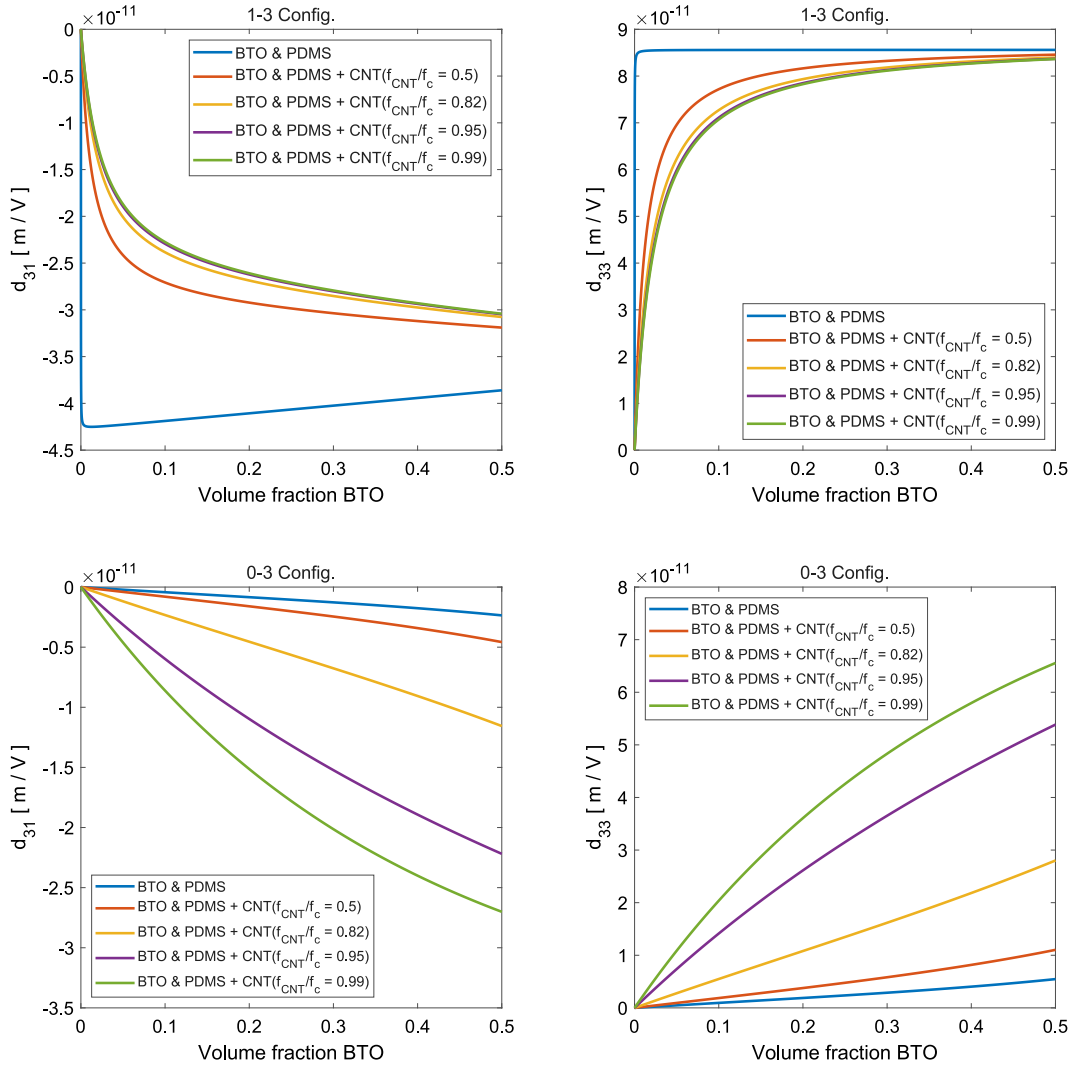

Fig. 11. Effective piezoelectric stress coefficients of BTO & PDMS piezocomposite: (a) d_{31} and (b) d_{33}, for different configurations (i.e., 1-3 and 0-3 configurations), as a function of the BTO volume fraction and the CNT volume fraction relative to the percolation threshold (f_{CNT}/f_c).

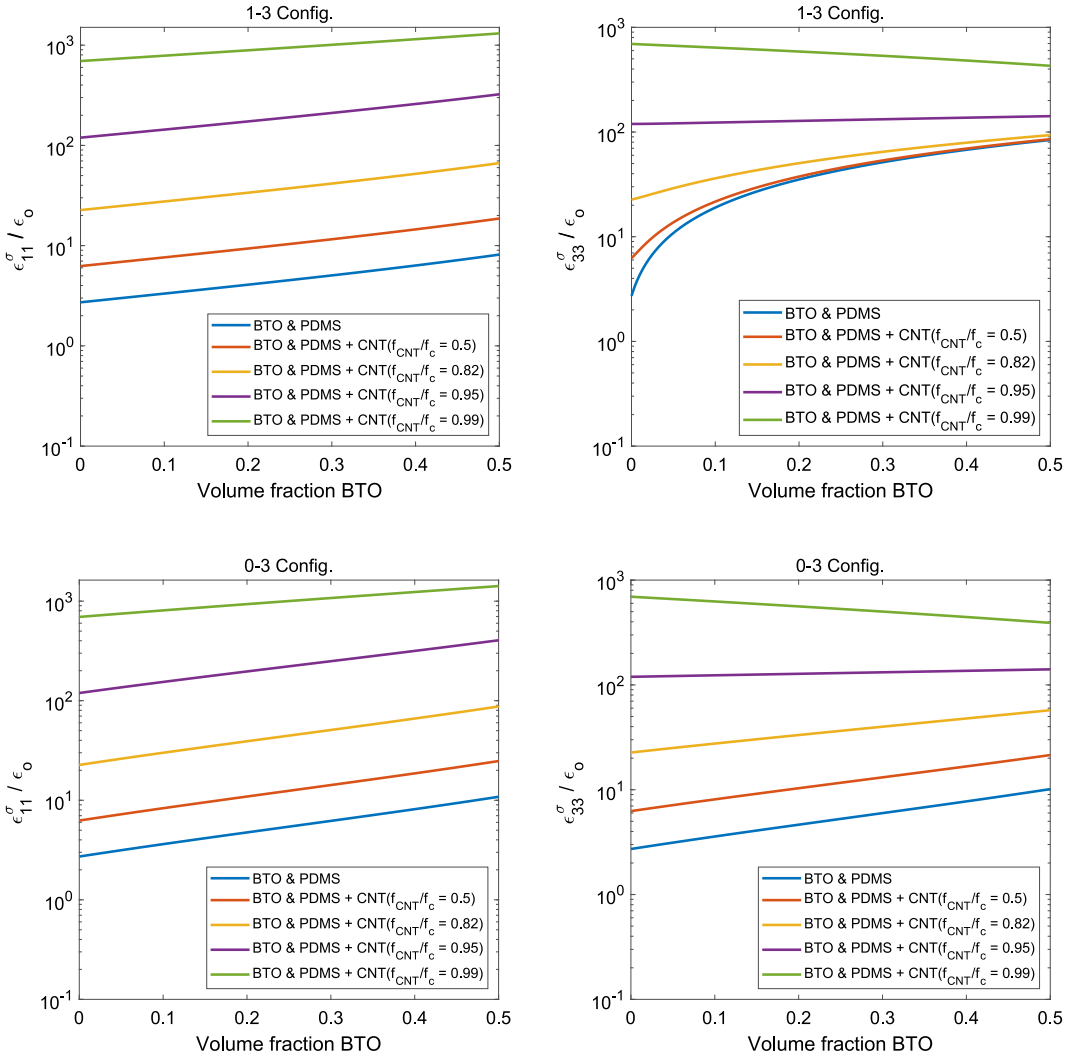

Fig. 12. Effective relative dielectric permittivities of the BTO & PDMS piezocomposite: (a) $\epsilon_{11}^{\sigma}/\epsilon_0$ and (b) $\epsilon_{33}^{\sigma}/\epsilon_0$, for different configurations (i.e., 1-3 and 0-3 configurations), as a function of the BTO volume fraction and the CNT volume fraction relative to the percolation threshold (f_{CNT}/f_c).

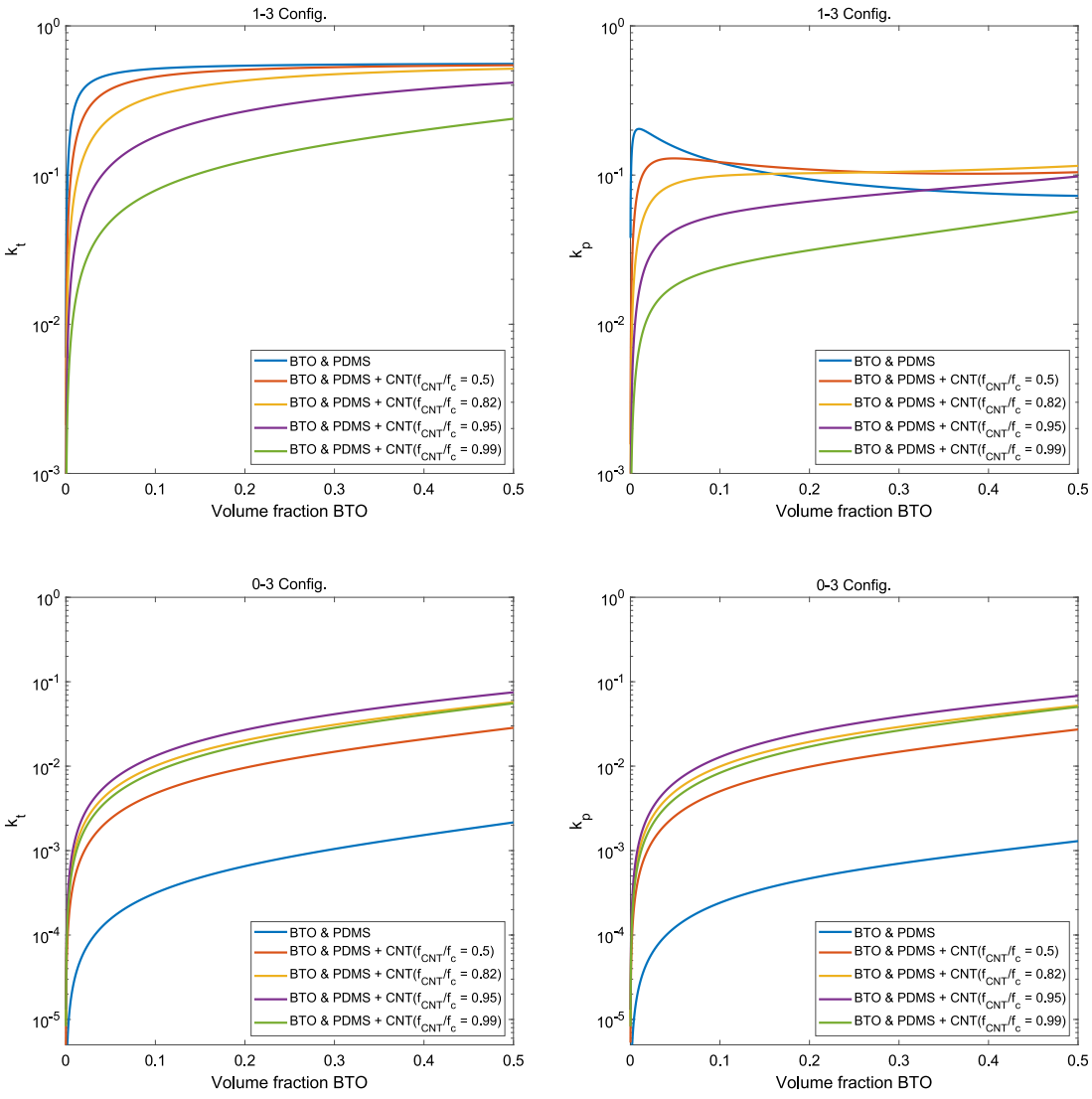

Fig. 13. Effective electromechanical coupling factors of the BTO & PDMS piezocomposite: (a) The thickness electromechanical coupling factor k_t for 1-3 and 0-3 configurations, and (b) the planar electromechanical coupling factor k_p for 1-3 and 0-3 configurations; as a function of the BTO volume fraction and the CNT volume fraction relative to the percolation threshold (f_{CNT}/f_c).

References

[1] Saito Y, Takao H, Tani T, Nonoyama T, Takatori K, Homma T, et al. Lead-free piezoceramics. Nature 2004;432:84–7.

[2] Hong Chang-Hyo, Kim Hwang-Pill, Choi Byung-Yul, Han Hyoung-Su, Son Jae Sung, Ahn Chang Won, et al. Lead-free piezoceramics – where to move on? J Materiomics 2016;2(1):1–24.

[3] Newnham RE, Skinner DP, Cross LE. Connectivity and piezoelectric-pyroelectric composites. Mater Res Bull 1978;13(5):525–36.

[4] Nan Ce-Wen. Physics of inhomogeneous inorganic materials. Prog Mater Sci 1993;37(1):1–116.

[5] Smith WA. The application of 1-3 piezocomposites in acoustic transducers. In: [Proceedings] 1990 IEEE 7th international symposium on applications of ferroelectrics. 1990, p. 145–52.

[6] Kumar A, Alih SF, Arockiarajan A. Energy harvesting from crystalline and conductive polymer composites. In: Ponnamma D, Sadasivuni KK, Cabibihan JJ, Al-Maadeed MA, editors. Smart polymer nanocomposites: energy harvesting, self-healing and shape memory applications. Cham: Springer International Publishing; 2017, p. 43–75.

[7] Cañamero FJ, Buroni FC, Aliabadi FMH, Rodríguez-Tembleque L. Piezoelectric performance of lead-free PDMS/CNT/$BaTiO_3$ piezocomposites with imperfect interphases and CNT agglomerations. Smart Mater Struct 2023;32(3):035005.

[8] Kim Kanguk, Zhu Wei, Qu Xin, Aaronson Chase, McCall William R, Chen Shaochen, et al. 3D optical printing of piezoelectric nanoparticle–polymer composite materials. ACS Nano 2014;8(10):9799–806.

[9] Yao Desheng, Cui Huachen, Hensleigh Ryan, Smith Parker, Alford Sam, Bernero Dominic, et al. Achieving the upper bound of piezoelectric response in tunable, wearable 3D printed nanocomposites. Adv Funct Mater 2019;29(42):1903866.

[10] Kabakov Peter, Kim Taeyang, Cheng Zhenxiang, Jiang Xiaoning, Zhang Shujun. The versatility of piezoelectric composites. Annu Rev Mater Res 2023;53(1):165–93.

[11] Chan HLW, Unsworth J. Simple model for piezoelectric ceramic/polymer 1-3 composites used in ultrasonic transducer applications. IEEE Trans Ultrason Ferroelectr Freq Control 1989;36(4):434–41.

[12] Dunn ML, Taya M. Micromechanics predictions of the effective electroelastic moduli of piezoelectric composites. Int J Solids Struct 1993;30(2):161–75.

[13] Dunn Martin L, Taya Minoru. An analysis of piezoelectric composite materials containing ellipsoidal inhomogeneities. Proc: Math Phys Sci 1993;443(1918):265–87.

[14] Poizat Christophe, Sester Matthias. Effective properties of composites with embedded piezoelectric fibres. Comput Mater Sci 1999;16(1):89–97.
[15] Levassort F, Topolov V Yu, Lethiecq M. A comparative study of different methods of evaluating effective electromechanical properties of 0–3 and 1–3 ceramic/polymer composites. J Phys D: Appl Phys 2000;33(16):2064.
[16] Odegard GM. Constitutive modeling of piezoelectric polymer composites. Acta Mater 2004;52(18):5315–30.
[17] Berger H, Kari S, Gabbert U, Rodriguez-Ramos R, Guinovart R, Otero JA, et al. An analytical and numerical approach for calculating effective material coefficients of piezoelectric fiber composites. Int J Solids Struct 2005;42:5692–714.
[18] Levin VM, Sabina FJ, Bravo-Castillero J, Guinovart-Díaz R, Rodríguez-Ramos R, Valdiviezo-Mijangos OC. Analysis of effective properties of electroelastic composites using the self-consistent and asymptotic homogenization methods. Internat J Engrg Sci 2008;46(8):818–34.
[19] de Medeiros Ricardo, Rodríguez-Ramos Reinaldo, Guinovart-Díaz Raul, Bravo-Castillero Julián, Otero José A, Tita Volnei. Numerical and analytical analyses for active fiber composite piezoelectric composite materials. J Intell Mater Syst Struct 2015;26(1):101–18.
[20] Isaeva Ashura N, Topolov Vitaly Yu. Lead-free 0–3-type composites: From piezoelectric sensitivity to modified figures of merit. J Adv Dielectr 2021;11(02):2150010.
[21] Isaeva Ashura N, Topolov Vitaly Yu. Comparative study on the performance of piezo-active 1–3-type composites with lead-free components. J Adv Dielectr 2021;11(05):2160003.
[22] Khan Kamran A, Hajeri Falah Al, Khan Muhammad Ali. Micromechanical modeling approach with simplified boundary conditions to compute electromechanical properties of architected piezoelectric composites. Smart Mater Struct 2021;30(3):035013.
[23] Topolov V Yu, Isaeva AN, Abramov PA. Effect of a heterogeneous matrix on piezoelectric and energy-harvesting parameters of modern lead-free 0–3 and quasi 1–3 composites. Ferroelectrics 2022;600(1):13–23.
[24] Krishnaswamy JA, Buroni FC, Garcia-Sanchez F, Melnik R, Rodriguez-Tembleque L, Saez A. Lead-free piezocomposites with CNT-modified matrices: Accounting for agglomerations and molecular defects. Compos Struct 2019;224:111033.
[25] Krishnaswamy JA, Buroni FC, Garcia-Sanchez F, Melnik R, Rodriguez-Tembleque L, Saez A. Improving the performance of lead-free piezoelectric composites by using polycrystalline inclusions and tuning the dielectric matrix environment. Smart Mater Struct 2019;28:075032.
[26] Krishnaswamy JA, Buroni FC, Garcia-Macias E, Melnik R, Rodriguez-Tembleque L, Saez A. Design of lead-free PVDF/CNT/BaTiO3 piezocomposites for sensing and energy harvesting: the role of polycrystallinity, nanoadditives and anisotropy. Smart Mater Struct 2020;29:015021.
[27] Krishnaswamy JA, Buroni FC, Garcia-Macias E, Melnik R, Rodriguez-Tembleque L, Saez A. Design of nano-modified PVDF matrices for lead-free piezocomposites: Graphene vs carbon nanotube nano-additions. Mech Mater 2020;142:103275.
[28] Krishnaswamy JA, Buroni FC, Melnik R, Rodriguez-Tembleque L, Saez A. Advanced modeling of lead-free piezocomposites: The role of nonlocal and nonlinear effects. Compos Struct 2020;238:111967.
[29] Krishnaswamy JA, Buroni FC, Melnik R, Rodriguez-Tembleque L, Saez A. Design of polymeric auxetic matrices for improved mechanical coupling in lead-free piezocomposites. Smart Mater Struct 2020;29:054002.
[30] Krishnaswamy JA, Rodriguez-Tembleque L, Melnik R, Buroni FC, Saez A. Size dependent electro-elastic enhancement in geometrically anisotropic lead-free piezocomposites. Int J Mech Sci 2020;182:105745.
[31] Krishnaswamy JA, Buroni FC, Melnik R, Rodriguez-Tembleque L, Saez A. Multiscale design of nanoengineered matrices for lead-free piezocomposites: Improved performance via controlling auxeticity and anisotropy. Compos Struct 2021;255:112909.
[32] Kim K, Zhu W, Qu X, Aaronson C, McCall WR, Chen S, et al. 3D optical printing of piezoelectric nanoparticle–polymer composite materials. ACS Nano 2014;8:9799–806.
[33] Sriphan S, Nawanil C, Vittayakorn N. Influence of dispersed phase morphology on electrical and fatigue properties of BaTiO3/PDMS nanogenerator. Ceram Int 2018;44:S38–42.
[34] Cañamero FJ, Buroni FC, Aliabadi FMH, Rodríguez-Tembleque L. Enhancing the performance of 1–3 lead-free piezoelectric composites using a CNT-doped matrix. J Multiscale Model 2023;14(2):2350003.
[35] Li JY. The effective electroelastic moduli of textured piezoelectric polycrystalline aggregates. J Mech Phys Solids 2000;48:529–52.
[36] Qiao Liao, Li Guo, Tao Hong, Wu Jiagang, Xu Zhuo, Li Fei. Full characterization for material constants of a promising KNN-based lead-free piezoelectric ceramic. Ceram Int 2020;46(5):5641–4.
[37] Mori T, Tanaka K. Average stress in matrix and average elastic energy of materials with misfitting inclusions. Acta Metall 1973;21:571–4.
[38] Bing J, Daining F. The effective properties of piezoelectric composite materials with transversely isotropic spherical inclusions. Appl Math Mech 1999;20:388–99.
[39] Huang Jin H, Yu JS. Electroelastic eshelby tensors for an ellipsoidal piezoelectric inclusion. Compos Eng 1994;4(11):1169–82.
[40] Mishra N, Das K. A mori–tanaka based micromechanical model for predicting the effective electroelastic properties of orthotropic piezoelectric composites with spherical inclusions. Compos Eng 2020;2:1206.
[41] European standard, EN 50324-2: (2002) Piezoelectric properties of ceramic materials and components, Part 2: Methods of measurement - Low power. Technical report, CENELEC European Committee for Electrotechnical Standardization; 2000.
[42] Johnston ID, McCluskey DK, Tan CKL, Tracey MC. Mechanical characterization of bulk sylgard 184 for microfluidics and microengineering. J Micromech Microeng 2014;24:035017.
[43] Roscow JI, Pearce H, Khanbareh H, Kar-Narayan S, Bowen CR. High temperature, high power piezoelectric composite transducers. Eur Phys J Spec Top 2019;228:1537–54.
[44] Bowen CR, Kim HA, Weaver PM, Dunn S. Piezoelectric and ferroelectric materials and structures for energy harvesting applications. Energy Environ Sci 2014;7:25–44.
[45] Li J, Ma PC, Chow WS, To CK, Tang BZ, Kim JK. Correlations between percolation threshold, dispersion state, and aspect ratio of carbon nanotubes. Adv Funct Mater 2007;17:3207–15.
[46] Bao H-D, Sun Y, Xiong Z-Y, Guo Z-X, Yu J. Effects of the dispersion state and aspect ratio of carbon nanotubes on their electrical percolation threshold in a polymer. Appl Polym Sci 2013;128:735–40.